

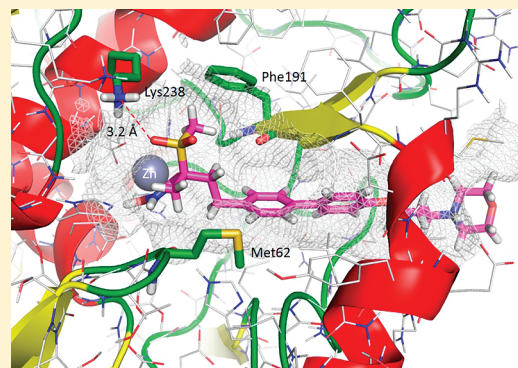
Potent Inhibitors of LpxC for the Treatment of Gram-Negative Infections

Matthew F. Brown,^{*,†} Usa Reilly,[†] Joseph A. Abramite,[†] Joel T. Arcari,[†] Robert Oliver,[†] Rose A. Barham,[†] Ye Che,[‡] Jinshan Michael Chen,[†] Elizabeth M. Collantes,[‡] Seung Won Chung,[†] Charlene Desbonnet,[§] Jonathan Doty,[†] Matthew Doroski,[†] Juntyma J. Engrakul,^{||} Thomas M. Harris,[†] Michael Huband,[§] John D. Knafels,[⊥] Karen L. Leach,^{||} Shenping Liu,[⊥] Anthony Marfat,[†] Andrea Marra,[§] Eric McElroy,[†] Michael Melnick,[†] Carol A. Menard,[#] Justin I. Montgomery,[†] Lisa Mullins,[§] Mark C. Noe,[†] John O'Donnell,[§] Joseph Penzien,[§] Mark S. Plummer,[†] Loren M. Price,[†] Veerabahu Shanmugasundaram,[‡] Christy Thoma,[§] Daniel P. Uccello,[†] Joseph S. Warmus,[†] and Donn G. Wishka[†]

[†]Worldwide Medicinal Chemistry, [‡]Computational Chemistry, [§]Antibacterials Research Unit, ^{||}Drug Metabolism, [⊥]Structural Biology, [#]Primary Pharmacology, Pfizer Global Research and Development, Eastern Point Road, Groton, Connecticut 06340, United States

S Supporting Information

ABSTRACT: In this paper, we present the synthesis and SAR as well as selectivity, pharmacokinetic, and infection model data for representative analogues of a novel series of potent antibacterial LpxC inhibitors represented by hydroxamic acid **1a**.



■ INTRODUCTION

Drug resistant Gram-negative infections are an increasing threat to public health, especially for seriously ill, hospitalized patients. Infections arising from multidrug resistant *Pseudomonas aeruginosa* and *Acinetobacter* species as well as carbapenem resistant *Klebsiella pneumoniae* present formidable challenges for the medical community as few treatment options remain.¹ Unfortunately, while resistance to current therapies continues to spread, new clinical agents to treat these infections are few in number.² In addition, the costs and regulatory challenges associated with the development of new antibacterial agents, combined with the perception of modest future profitability, has unfortunately resulted in most major pharmaceutical companies exiting anti-infective drug research at a time when it is most needed.³

While it has been regularly stated that there is a great need to identify novel lead series with new antibacterial modes of action, in reality this goal remains highly elusive. A 2007 paper from GlaxoSmithKline nicely illustrates this challenge as a meager five lead series were identified from 67 target-based high-throughput screens conducted over a 7 year period.⁴ Inhibition of cell wall biosynthesis is a well-precedented anti-infective strategy (i.e., β -lactams), and efforts to identify novel targets essential to cell wall biosynthesis in Gram-negative bacteria have been reported.⁵ Gram-positive bacteria contain both a cytoplasmic inner membrane

and an outer membrane composed of peptidoglycan. In addition to these membranes, Gram-negative bacteria possess an additional outer membrane decorated with lipopolysaccharide (LPS). LPS is composed of three distinct units. The outermost unit is the O-antigen, which is a glycan polymer. This is linked to a sugar-containing core domain which is appended to the membrane anchoring group, lipid A (endotoxin). This outer membrane provides a substantial protective barrier, and Gram-negative bacteria lacking lipid A are either not viable or are highly susceptible to a range of anti-infective drugs, suggesting that enzymes involved in lipid A production could represent new drug targets.⁶ Nine unique enzymes catalyze the synthesis of lipid A and UDP-3-O-(R-3-hydroxymyristol)-N-acetylglucosamine deacetylase (LpxC) is a cytosolic zinc-metalloamidase responsible for carrying out the second biosynthetic step.⁷ The essential role LpxC plays in the biosynthesis of lipid A, coupled with a lack of homology with mammalian proteins, has catalyzed efforts to identify small molecule LpxC inhibitors for the treatment of serious Gram-negative infections.

Inhibitors were first disclosed by researchers at Merck in the 1990s (e.g., L-161,240, Figure 1),⁸ and this was followed by a

Received: November 1, 2011

Published: December 18, 2011

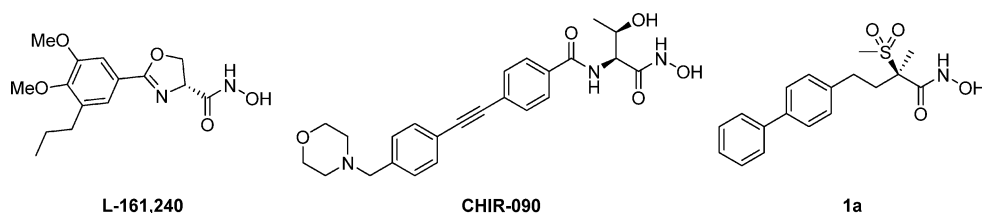
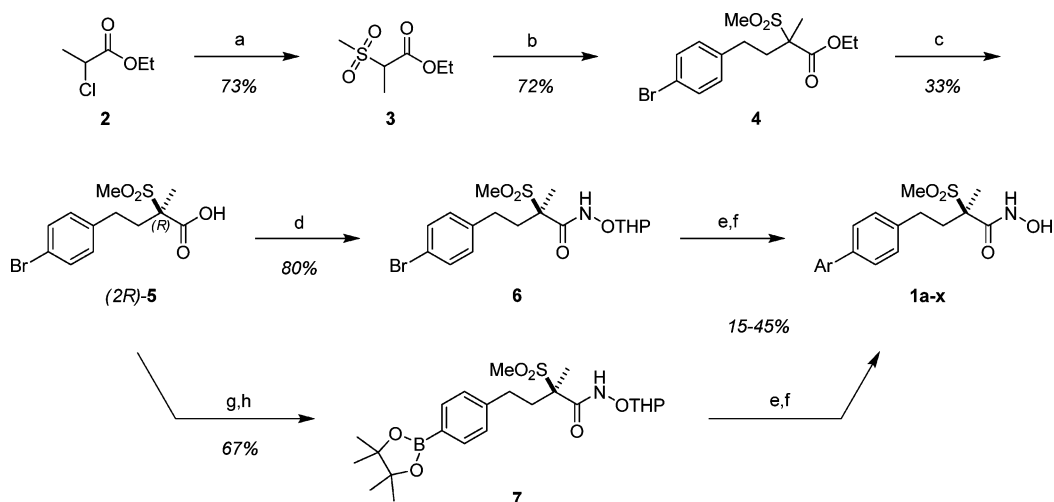


Figure 1. LpxC inhibitors.

Scheme 1. General Preparation of Biaryl Analogues 1^a

^aReagents and conditions: (a) NaSO₂Me, EtOH, reflux; (b) 1-bromo-4-(2-bromoethyl)benzene, Cs₂CO₃, DMF; (c) (i) LiOH, THF, MeOH, H₂O, (ii) classical resolution using (–)-ephedrine, IPA, H₂O; (d) CDMT, NMM, NH₂OTHP, 2-MeTHF; (e) ArB(OH)₂ or ArBr, Pd(II) EnCat, K₂CO₃, EtOH, H₂O, 80 °C; (f) HCl 1,4-dioxane, H₂O; (g) bis(pinacolato)diborane, Pd(dppf)Cl₂, KOAc, 1,4-dioxane, 100 °C; (h) HOBT, Et₃N, NH₂OTHP, EDCl, CH₂Cl₂.

variety of reports describing inhibitors with improved enzyme potency and antibacterial spectrum, with CHIR-090 being one of the most extensively studied inhibitors.⁹ Crystallography and NMR studies have provided a wealth of information regarding LpxC protein conformation as well as the binding mode of various small molecule inhibitors at the active site.¹⁰ L-161,240, CHIR-090, and other inhibitors described in the literature are structurally similar in that they contain a zinc-binding group (e.g., hydroxamic acid) and a hydrophobic tail which mimics the hydroxy-myristate fatty acid group found in the natural enzyme substrate. These lipophilic moieties make important van der Waals interactions with the enzyme in a hydrophobic tunnel, which are critical for potent enzyme inhibition. Here, we provide initial details regarding a novel series of alkyl hydroxamic acid LpxC inhibitors, exemplified by compound 1a (Figure 1). The potent activity exemplified by this series can, in part, be attributed to an important hydrogen-bonding interaction between the alkylsulfone headgroup and a lysine residue located near the catalytic site (Lys238).

CHEMISTRY

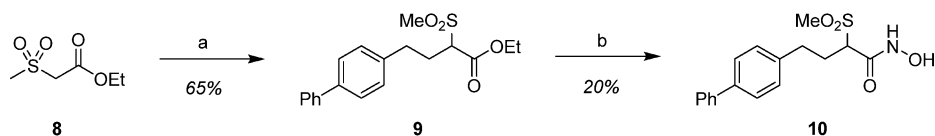
The majority of the LpxC inhibitors that are described within are biaryl derivatives (1a–x), and these were prepared in short order from templates 6 and 7, as illustrated in Scheme 1. Treatment of chloride 2 with sodium methanesulfinate in refluxing ethanol provided the methylsulfone 3, which was alkylated with 1-bromo-4-(2-bromoethyl)benzene under basic conditions to provide ester 4. Saponification of 4 provided the acid 5, as a racemic mixture, that was subjected to a classical resolution with (–)-ephedrine. Single crystal X-ray structures of

each enantiomer (2R)-5 and (2S)-5 were obtained to assign the absolute stereochemistry. The preferred (2R)-5 enantiomer, which provides the more active hydroxamic acid analogues 1, was converted to the phenyl bromide template 6 under standard amide coupling conditions with *O*-(tetrahydro-2H-pyran-2-yl)hydroxylamine (NH₂OTHP). The boronate ester template 7 was prepared in a two-step sequence from 5 involving a palladium-catalyzed cross-coupling reaction with bis(pinacolato)diborane followed by an amide formation with NH₂OTHP. Templates 6 and 7 were subjected to Suzuki–Miyaura cross coupling reactions with aryl boronic acids and aryl bromides, respectively, and subsequent acid-mediated deprotections to provide the desired hydroxamic acids 1a–x.

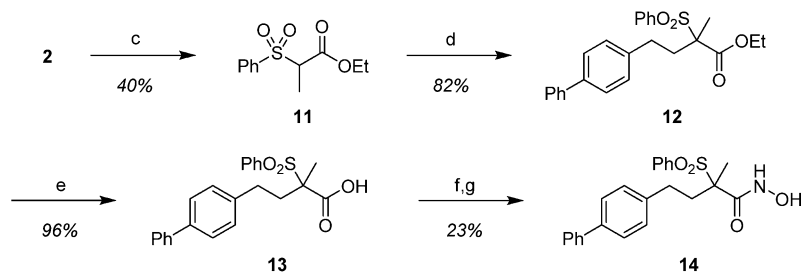
The biphenyl analogues 10, 14, and 17, and generally all analogues described herein, were prepared in a similar fashion to that of 1a–x whereby incorporation of the hydrophobic tail is achieved through alkylation of a sulfone ester moiety. For example, treatment of methylsulfone 8 with sodium hydride and 4-(2-bromoethyl)biphenyl provided ester 9, which was converted to the hydroxamic acid 10 under direct amidation conditions with hydroxylamine hydrochloride (Scheme 2). The phenylsulfone 11, prepared in a similar fashion to that of methylsulfone 3, was treated with cesium carbonate and 4-(2-iodoethyl)biphenyl to provide the biphenyl intermediate 12. After basic hydrolysis, the corresponding free acid (13) was converted to the hydroxamic acid 14. Likewise, the sulfolane derivative 15 was alkylated under basic conditions with 4-(2-iodoethyl)biphenyl to provide ester 16, which was transformed using standard hydrolysis/amidation/deprotection procedures to the desired hydroxamic acid 17.

Scheme 2. Synthesis of Biphenyl Analogues 10, 14, and 17^a

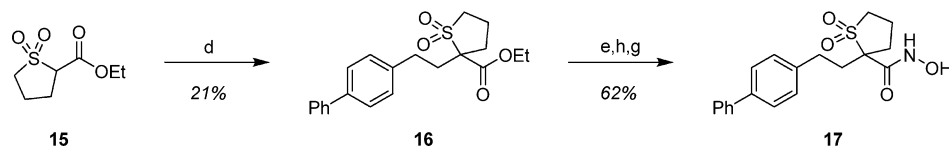
Preparation of 10:



Preparation of 14:



Preparation of 17:

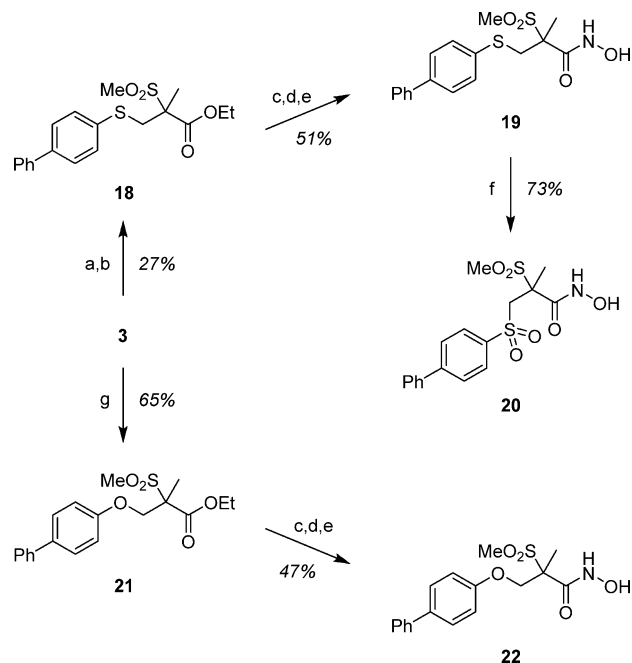


^aReagents and conditions: (a) (i) NaH, DMF, 0 °C; (ii) 4-(2-bromoethyl)biphenyl, 0 °C to rt; (b) NH₂OH·HCl, NaOMe, MeOH, THF, 0 °C to rt; (c) NaSO₂Ph, EtOH, reflux; (d) 4-(2-iodoethyl)biphenyl, Cs₂CO₃, DMF; (e) LiOH, THF, MeOH, H₂O; (f) CDMT, NMM, NH₂OTHP, 2-MeTHF; (g) HCl, 1,4-dioxane, H₂O; (h) NH₂OTHP, PyBOP, DIPEA, CH₂Cl₂.

The preparation of analogues 19, 20, and 22, containing heteroatoms linking the biaryl tail group to the hydroxamate headgroup, is shown in Scheme 3. Deprotonation of sulfone 3 with lithium hexamethyldisilazide (LiHMDS), followed by treatment with (4-bromophenyl)-(chloromethyl)sulfane, furnished an arylbromide intermediate that was coupled with phenyl boronic acid under typical Suzuki–Miyaura conditions to provide ester 18. Hydrolysis, amide coupling with NH₂OTHP, and acid-promoted deprotection of 18 led to the hydroxamic acid 19, which was oxidized to the sulfone 20 with oxone. Compound 22 was produced in a similar fashion, whereby 3 was first alkylated with 4-(chloromethoxy)biphenyl to provide ether 21, which was then converted by the same sequence of reactions to the hydroxamic acid 22.

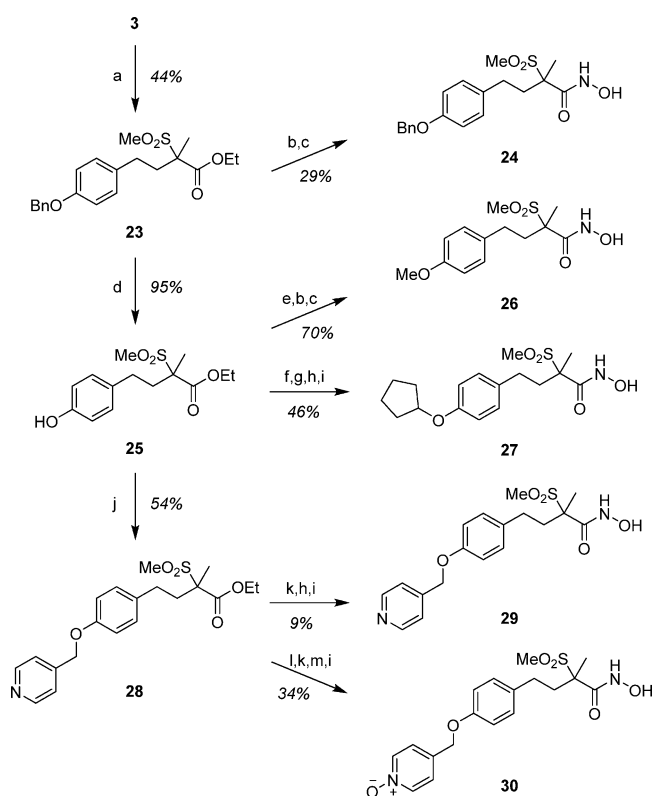
A variety of methods were utilized to prepare the phenyl ether analogues 24, 26, 27, 29 and 30, as illustrated in Scheme 4. The alkylation of sulfone 3 with 1-(benzyloxy)-4-(2-iodoethyl)benzene under basic conditions provided ester 23, which upon saponification was converted to the hydroxamic acid 24, as previously described. Hydrogenolysis of 23 with Pearlman's catalyst and cyclohexene provided the common phenol intermediate 25. Methylation of 25, followed by conversion of the ester moiety to the hydroxamic acid in the usual manner, produced 26. Mitsunobu reactions were employed to install the cyclopentyl and (4-pyridyl)methyl groups of 27 and 29, respectively, and an *m*CPBA oxidation of the (4-pyridyl)methyl group of 28 ultimately led to the (4-pyridinyl)methyl *N*-oxide 30. In general, the hydroxamic acid moieties of these analogues were introduced in a similar fashion (ester hydrolysis, amide bond formation, and an acidic deprotection).

The thioether analogue 33 was prepared from the enantiopure acid 5, beginning with the conversion to the methyl ester via alkylation with methyl iodide (Scheme 5).

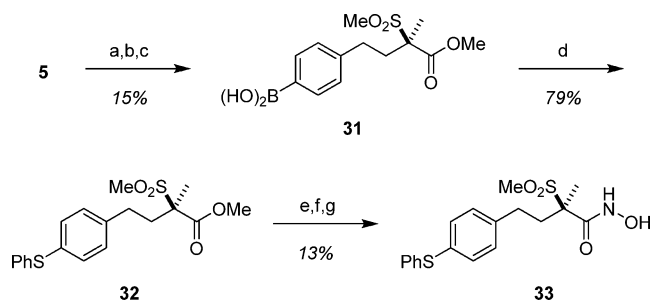
Scheme 3. Synthesis of biphenyl analogues 19, 20, and 22^a

^aReagents and conditions: (a) (i) LiHMDS, THF, NMP, 0 °C, (ii) (4-bromophenyl)-(chloromethyl)sulfane, NaI, 0 °C to rt; (b) PhB(OH)₂, Pd(PPh₃)₄, K₂CO₃, 1,4-dioxane, H₂O, 80 °C; (c) NaOH, 1,4-dioxane, H₂O; (d) (i) CDMT, NMM, 2-MeTHF, (ii) NH₂OTHP; (e) PPTS, EtOH; (f) oxone, MeOH, H₂O; (g) (i) NaH, DMP, 0 °C, (ii) 4-(chloromethoxy)biphenyl, NaI, 0 °C to rt.

A palladium-catalyzed cross-coupling with bis(pinacolato)diborane provided the pinacol boronate ester, which was then

Scheme 4. Synthesis of Phenyl Ether Analogues 24, 26, 27, 29, and 30^a

^aReagents and conditions: (a) 1-(benzyloxy)-4-(2-iodoethyl)benzene, Cs_2CO_3 , DMF, 50 °C; (b) LiOH, THF, MeOH, H_2O ; (c) (i) oxalyl chloride, DMF, DCM, (ii) NH_2OTMS ; (d) $\text{Pd}(\text{OH})_2/\text{C}$, cyclohexene, EtOH, reflux; (e) MeI, Cs_2CO_3 , DMF; (f) cyclopentanol, PPh_3 , DIAD, THF, 0 °C to rt; (g) NaOH, 1,4-dioxane, H_2O ; (h) (i) CDMT, NMM, 2-MeTHF, (ii) NH_2OTHP ; (i) PPTS, EtOH; (j) pyridin-4-ylmethanol, PPh_3 , DIAD, THF, 0 °C to rt; (k) KOH, 2-MeTHF, H_2O , 60 °C; (l) *m*CPBA, HOAc, 55 °C; (m) propylphosphonic anhydride, Et_3N , NH_2OTHP , 2-MeTHF.

Scheme 5. Synthesis of Thioether Analogue 33^a

^aReagents and conditions: (a) MeI, NaHCO_3 , THF, H_2O ; (b) bis(pinacolato)diborane, $\text{Pd}(\text{dppf})\text{Cl}_2$, KOAc, 1,4-dioxane, 100 °C; (c) NaIO_4 , NH_4OAc , acetone, H_2O ; (d) phenyl disulfide, CuI, 2,2'-bipyridine, DMSO, H_2O , 100 °C; (e) NaOH, 1,4-dioxane, H_2O ; (f) HOBt, Et_3N , NH_2OTHP , EDCl, CH_2Cl_2 ; (g) HCl, MeOH, 1,4-dioxane, H_2O .

subjected to oxidative conditions to furnish the boronic acid **31**. The copper-mediated cross coupling of **31** with phenyl disulfide provided the thioether ester **32**, which was transformed to the final target **33**, as previously described.

RESULTS AND DISCUSSION

A novel structural feature of the series reported here is the alkyl-linked sulfone-containing headgroup, which differs from the amide-linked threonine-containing headgroup found in CHIR-090 and related inhibitors. The sulfone moiety is engaged in a hydrogen-bonding interaction with Lys238, an interaction maintained by the threonine hydroxyl group common to the CHIR-090-like inhibitors (Figure 2). The methyl group attached

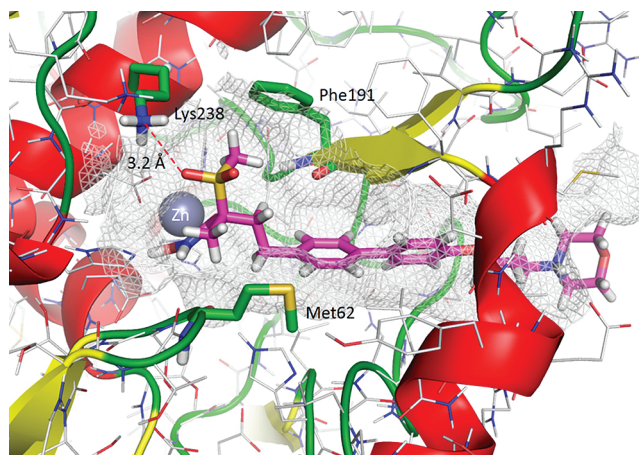
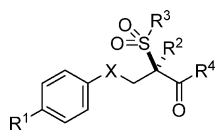


Figure 2. X-ray crystal structure of **1t** with *Pseudomonas aeruginosa* LpxC enzyme.

to the sulfone resides in a fairly small hydrophobic space defined by a cluster of phenylalanine residues, the closest being Phe191; a similar van der Waals interaction is observed for the threonine methyl group of the CHIR-090 analogues. This space will not accommodate larger substituents. For example, the corresponding analogue wherein the sulfone methyl group of **1a** has been replaced by the larger phenyl group (Table 1, compound **14**) is significantly less potent than **1a** in the *Pseudomonas aeruginosa* LpxC enzyme assay (PaeLpxC). While a simple bond rotation would place the phenyl group in solvent exposed space and still enable interaction of a sulfone oxygen with Lys238, the loss in potency suggests that this conformation is not optimal, perhaps due to the placement of the polar sulfone oxygens in the region of the hydrophobic phenylalanine cluster, as well as the loss of the van der Waals interaction present with the methyl-containing analogue **1a**. Interestingly, locking the sulfone moiety into a ring as shown in compound **17** also leads to a significant loss of enzyme activity, which may again be explained by an unfavorable placement of the sulfone oxygens near the phenylalanine cluster. Enzyme inhibitory activity in this series resides with analogues with (*R*) absolute stereochemistry (compare (*R*) enantiomer **1a** (1.37 nM) to (*S*) enantiomer (*S*)-**1a** (>95.2 nM)). While the binding site appears capable of accommodating both configurations, compounds in the (*S*) configuration place the methylsulfone group into solvent-exposed space, thus losing the interaction with Lys238. This result demonstrates that maintaining this H-bonding interaction is critical for achieving significant potency in this series. The methyl group appended to the quaternary center in compound **1a** is located in a generally solvent exposed region, perhaps making a positive van der Waals contact with a nearby Met62. Racemic compound **10**, the des-methyl analogue of compound **1a**, shows an approximate 10-fold loss of enzyme potency relative to **1a**. The absence of substitution at this

Table 1. LpxC Inhibitors^a

Cmpd	X	R1	R2	R3	R4	PaeLpxC	MIC (μg/mL)		clogD ^b
						IC ₅₀ (nM)	PAO1	SA21	
Cipro ^c	-	-	-	-	-	-	0.125	0.25	-0.73
CHIR-090	-	-	-	-	-	< 2.05 ± 0.84	1	>64	1.1
1a	-CH ₂ -	Ph	Me	Me	NHOH	1.37 ± 0.71	0.125	>64	2.2
(S)-1a ^d	-CH ₂ -	Ph	Me	Me	NHOH	> 95.2 ± 8.31	>64	>64	2.2
10 ^e	-CH ₂ -	Ph	H	Me	NHOH	13.8 ± 2.36	1	>64	1.8
14 ^e	-CH ₂ -	Ph	Me	Ph	NHOH	> 67.9 ± 40.3	64	32	3.9
17 ^e	-CH ₂ -	Ph	-(CH ₂) ₃ -		NHOH	> 92.5 ± 13.0	>64	64	1.6
19 ^e	-S-	Ph	Me	Me	NHOH	9.04 ± 4.39	2	64	2.4
20 ^e	-SO ₂ -	Ph	Me	Me	NHOH	11.9 ^f	4	>64	1.3
22 ^e	-O-	Ph	Me	Me	NHOH	31.4 ± 19.7	4	>64	1.8
1b	-CH ₂ -		Me	Me	NHOH	1.36 ± 0.76	0.125	32	2.7
1c	-CH ₂ -		Me	Me	NHOH	7.04 ± 0.01 ^g	1	>64	1.8
1d	-CH ₂ -		Me	Me	NHOH	26.1 ± 8.98	8	32	3.2
1e	-CH ₂ -		Me	Me	NHOH	>100	>64	>64	0.4
1f	-CH ₂ -		Me	Me	NHOH	3.54 ± 2.91	0.5	32	2.7
1g	-CH ₂ -		Me	Me	NHOH	6.78 ± 3.93	8	32	3.5
1h	-CH ₂ -		Me	Me	NHOH	22.1 ± 7.07	32	64	2.1
1i	-CH ₂ -		Me	Me	NHOH	27.8 ± 5.02	32	>64	0.7
1j	-CH ₂ -		Me	Me	NHOH	< 1.05 ± 0.56	0.5	16	2.7

Table 1. continued

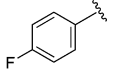
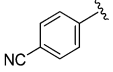
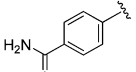
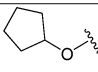
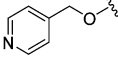
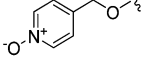
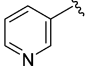
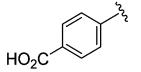
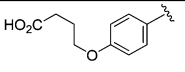
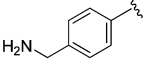
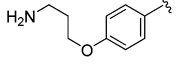
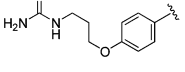
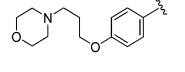
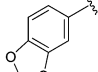
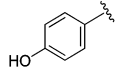
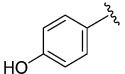
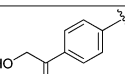
Cmpd	X	R1	R2	R3	R4	PaeLpxC		MIC ($\mu\text{g/mL}$)		clogD^b
						IC_{50} (nM)	PAO1	SA21		
1k	-CH ₂ -		Me	Me	NHOH	1.74 ± 1.06	0.25	>64	2.1	
1l	-CH ₂ -		Me	Me	NHOH	0.64 ± 0.37	0.125	>64	1.5	
1m	-CH ₂ -		Me	Me	NHOH	$< 2.47 \pm 1.84$	2	>64	0.6	
34	-CH ₂ -	-H	Me	Me	NHOH	> 100	16	>64	0.4	
24 ^e	-CH ₂ -	-OBn	Me	Me	NHOH	5.16 ± 1.46	2	>64	2.0	
26 ^e	-CH ₂ -	-OMe	Me	Me	NHOH	> 100	16	>64	0.3	
27 ^c	-CH ₂ -		Me	Me	NHOH	10.1 ± 1.02	4	64	1.8	
29 ^e	-CH ₂ -		Me	Me	NHOH	21.6 ± 6.47	4	>64	0.5	
30 ^c	-CH ₂ -		Me	Me	NHOH	92.7 ± 51.5	>64	>64	-1.4	
33	-CH ₂ -	-SPh	Me	Me	NHOH	30.4 ± 4.03	4	64	2.6	
1n	-CH ₂ -		Me	Me	NHOH	29.7 ± 20.4	4	>64	0.8	
1o	-CH ₂ -		Me	Me	NHOH	73.6 ± 22.8	64	>64	-0.9	
1p	-CH ₂ -		Me	Me	NHOH	21.2 ± 13.4	8	>64	-0.6	
1q	-CH ₂ -		Me	Me	NHOH	12.9 ± 2.42	1	>64	-0.9	
1r ^e	-CH ₂ -		Me	Me	NHOH	12.7 ± 6.02	2	>64	-0.7	
1s ^c	-CH ₂ -		Me	Me	NHOH	9.49 ± 3.66	32	32	-0.9	
1t	-CH ₂ -		Me	Me	NHOH	$< 2.13 \pm 1.72$	2	>64	1.4	
1u	-CH ₂ -		Me	Me	NHOH	1.20 ± 0.58	0.125	>64	2.0	

Table 1. continued

Cmpd	X	R1	R2	R3	R4	PaeLpxC		MIC ($\mu\text{g/mL}$)		clogD ^b
						IC ₅₀ (nM)	PAO1	SA21		
1v	-CH ₂ -		Me	Me	NHOH	3.68 ± 1.42	0.5	>64	1.4	
1w	-CH ₂ -		Me	Me	CO ₂ H	> 92.5 ± 13.0	>64	>64	-0.9	
1x	-CH ₂ -		Me	Me	NHOH	1.85 ± 0.99	0.5	>64	0.5	

^aAnalogues are (*R*)-enantiomers unless otherwise indicated. ^bclogD calculated at pH 7.4 with ACD pchbat version 9.3. ^cCiprofloxacin. ^d(*S*)-enantiomer. ^eracemic. ^f*n* = 1 data. ^g*n* = 2 data.

center may allow racemization to occur with isolated enantiomers due to the acidic nature of the methine proton. Therefore, in addition to van der Waals interactions, the methyl group found in **1a** could play an important role of locking the molecule in the more potent (*R*) stereochemical configuration.

The composition of the tether group linking the sulfone headgroup to the biphenyl moiety was briefly explored. The two-carbon linker found in **1a** is preferred while analogues with the thioether (**19**), sulfone (**20**), and ether linkages (**22**) retain reasonable potency. Of this set, the ether linked analogue **22** is least potent. The preferred C-CH₂-O-C_{ar} torsion angle for ether analogue **22** would be expected to be close to 0°,¹¹ quite different from the angle observed in the crystal structures for the ethylene-linked analogues (Figure 2). As observed with literature LpxC inhibitors, the hydroxamic acid in our series interacts with the active-site zinc in a chelating fashion and the aryl tailgroup occupies the enzymatic hydrophobic tunnel. The hydroxamic acid is an efficient zinc-binding group, and replacement of this moiety with a carboxylic acid also capable of binding zinc leads to significantly diminished potency (compare hydroxamic acid **1v** (3.68 nM) with carboxylic acid **1w** (>92.5 nM)). The morpholino group appended to the 4-position of the terminal aryl ring in compound **1t** exits the end of the hydrophobic tunnel and resides in solvent-exposed space (Figure 2).

It has been reported in the literature that the moiety linked to the zinc-binding headgroup needs to be a hydrophobic group of adequate length to efficiently interact with the hydrophobic tunnel and maintain reasonable potency.^{8,9c} Therefore, removal of the terminal aryl ring of compound **1a** leads to significantly diminished enzymatic potency (compound **34**, >100 nM). Adding a 4-methoxy group to the aryl ring offers no improvement (**26**), however, a variety of other analogues with various oxygen or sulfur-linked lipophilic groups provide a significant boost in potency relative to **34** and **26** (e.g., **24**, **27**, **29** and **33**). Generally speaking, the biphenyl tailgroup present in compound **1a** provides the highest level of potency and antibacterial spectrum, therefore, the effect of terminal ring substitution of the biaryl group was extensively explored.

Direct attachment of polar functionality at the 2-position of the terminal ring as shown with amide **1e** leads to significantly reduced enzymatic and cellular potency due to the desolvation cost associated with placement of polar functionality in the LpxC hydrophobic tunnel. In addition, the 2-position is tolerant to small, lipophilic functional groups. However, activity

is reduced as the size of this group is increased. For example, the 2-ethyl analogue **1d** is 19-fold less potent than the des-ethyl analogue **1a**. A similar trend is observed at the 3-position, however, this position is more tolerant to varying size and polarity as compared to the 2-position. With its placement near the mouth of the hydrophobic tunnel, the 4-position of the terminal aryl ring is tolerant to a wider range of functionality, and attachment of a variety of groups at this position results in single-digit nM enzyme inhibitors with impressive anti-*Pseudomonas* whole-cell activity (**1j–m**, **1u**, **1v**, **1x**). For example, while placement of a polar primary amide at the 2- or 3-positions leads to diminished potency relative to **1a**, the 4-amide analogue **1m** demonstrates equivalent enzymatic activity. A variety of analogues with basic functionality at the 4-position show decent enzyme inhibition (**1q–1t**), however, the guanidine-containing analogue **1s** is substantially less active than the other amine-containing analogues with regard to whole-cell activity. The benzoic acid analogue **1o** shows rather weak enzymatic activity, however, addition of an alkylether linkage to place the polar acidic functionality in solvent exposed space outside of the hydrophobic tunnel provides a moderate improvement in potency (**1p**).

Replacement of the terminal aryl ring of compound **1a** with a variety of heteroaryl groups typically provides reduced potency. For example, the pyridyl analogue **1n** shows an approximate 20-fold loss of enzymatic potency as compared to **1a**. A number of literature inhibitors, including CHIR-090, link a biphenyl acetylene moiety to the zinc-binding headgroup to achieve optimal potency. Given the safety concerns associated with mechanism-based inactivation of cytochrome P450 enzymes mediated by alkyne-containing drugs,¹² it is noteworthy that high-level enzyme potency and whole-cell activity is achieved in this series in the absence of an arylacetylene.

The ability to append a range of functional groups at the 4-position of the terminal aryl ring provides the potential to fine-tune molecular properties. That said, analogues in this series with relatively low clogD values generally demonstrate reduced enzymatic and cellular potency. For example, the highly polar *N*-oxide found in compound **30** (clogD -1.4) is located in solvent exposed space, yet this molecule is 4-fold less potent than the corresponding pyridine **29** (clogD 0.5) in the enzyme assay and ≥16-fold less active in the cell-based assay. This trend has been generally observed in this series as molecules with low clogD values (<0) regularly show reduced enzymatic and whole-cell potency. Conversely, compounds from this series

Table 2. MIC₉₀ Values for Select Analogues

strains	n	MIC ₉₀ (μg/mL)									
		cipro	Azt	CHIR-090	1a	1k	1l	1t	1u	1v	1x
<i>Pseudomonas aeruginosa</i>	22	64	64	4	4	1	1	4	1	2	1
<i>Klebsiella pneumoniae</i>	22	64	>64	2	16	8	2	4	4	16	8
<i>Escherichia coli</i>	11	>64	>64	0.25	2	1	0.5	0.5	0.5	4	2
<i>Enterobacter aerogenes</i>	11	1	32	0.5	4	2	1	1	1	16	4
<i>Citrobacter freundii</i>	11	32	>64	0.5	8	4	2	1	2	8	4
<i>Acinetobacter baumannii</i>	11	64	32	>64	32	32	16	>64	>64	>64	>64

with relatively high clogD values (>3) occasionally demonstrate Gram-positive antibacterial whole-cell activity (*Staphylococcus aureus* strain SA21 (ATCC 29213), Table 1), suggesting the potential for off-target activity because Gram-positive bacteria lack LpxC enzyme. Therefore, analogue design efforts were focused within polarity space (clogD ~ 0–3) to provide optimal enzymatic and Gram-negative whole-cell activity while minimizing Gram-positive activity. While oxidative metabolism is not the major contributor to drug clearance in this series (vide infra), focusing design at the lower end of this clogD scale also reduced the extent of oxidative metabolism observed in liver microsome incubations (unpublished results).

Micromolar whole-cell activity is common for Gram-negative drug research programs and highlights the formidable cellular barriers and resistance mechanisms present in these pathogens. Given that drugs with cytosolic targets must pass through the rather impenetrable outer membrane as well as the inner membrane, while avoiding a number of multidrug resistant efflux pumps to reach their biological targets,¹³ it is remarkable that effective bacterial killing is ever achieved. The relative impact of efflux on whole-cell activity can be illustrated by determining the MIC shift that occurs for compound **1a** when comparing data from the wild-type *Pseudomonas aeruginosa* strain PA01 (MIC = 0.125 μg/mL = 0.37 μM) to a PA01-modified strain (PAO280) which lacks major efflux pumps ($\Delta(mexAB-OprM) \Delta(mexXY)\Delta(MexZ)$) (MIC = 0.008 μg/mL = 23 nM).¹⁴ The magnitude of the efflux-mediated MIC shift illustrated by this example (~ 16-fold) is consistently observed with analogues in this series.

Having identified potent PaeLpxC enzyme inhibitors with whole-cell activity, MIC₉₀ values were obtained for select compounds vs a panel of important Gram-negative pathogens, including *Pseudomonas aeruginosa*, *Klebsiella pneumoniae*, *Escherichia coli*, *Enterobacter aerogenes*, *Citrobacter freundii*, and *Acinetobacter baumannii* (Table 2). The LpxC inhibitors (CHIR-090 included) significantly outperform the comparator agents ciprofloxacin and aztreonam with the exception that ciprofloxacin demonstrates similar activity vs *Enterobacter aerogenes*. None of the compounds evaluated in this study exhibit significant activity vs *Acinetobacter baumannii*. In general, the LpxC inhibitors described here exhibit diminished *Acinetobacter* LpxC enzyme activity as compared to PaeLpxC, leading to relatively weak whole-cell *Acinetobacter* activity.

Analogues **1a** and **1v** were further profiled against a larger panel of 91 clinically relevant strains of *Pseudomonas aeruginosa*. Phenol **1v** was selected for this advanced evaluation based on solid activity observed in the small panel study described above, combined with the ability to utilize the phenol as a prodrug handle to maximize aqueous solubility in future in vivo studies. Both compounds demonstrate impressive MIC₉₀ values of 2 and 4 μg/mL (Table 3). The LpxC inhibitors show superior activity to all the comparator drugs in this study with the

Table 3. MIC₉₀ Data vs 91 Strains of *Pseudomonas aeruginosa*

compd	range (μg/mL)	MIC ₅₀ (μg/mL)	MIC ₉₀ (μg/mL)
1a	0.008–4	0.5	2
1v	0.015–8	1	4
ciprofloxacin	0.008 to >64	2	32
amikacin	0.5 to >64	4	32
polymyxin B	0.25–2	0.5	1
cefepime	0.25 to >64	16	64
ceftazidime	1 to >64	16	>64

exception of polymyxin B, which is considered to be a drug of last resort for the treatment of multidrug resistant *Pseudomonas aeruginosa* infections due to its considerable toxicity.

Given the structural similarity of this series of LpxC inhibitors to known hydroxamic acid MMP inhibitors, compound **1a** was also evaluated against a panel of metalloproteases. Good selectivity was observed except for two targets showing K_i values <10 μM (MMP12 and MMP13, Table 4). The selectivity

Table 4. MMP Activity for **1a**

hMMPs	K_i (μM)	hMMPs	K_i (μM)
MMP1	>10	MMP14	>10
MMP2	>10	MMP15	>10
MMP3	>10	MMP16	>10
MMP7	>10	MMP20	>10
MMP8	>10	MMP24	>10
MMP9	>10	MMP25	>10
MMP10	>10	MMP26	>10
MMP12	1.35	TACE	>10
MMP13	7.73		

of compound **1a** was also determined against a panel of 120 targets at a 10 μM drug concentration.¹⁵ Minimal off-target activity was observed as >50% inhibition was only obtained in two instances; human norepinephrine (NE) transporter (IC₅₀ = 340 nM, K_i = 250 nM) and PDE11 (IC₅₀ = 18 μM).

Hydroxamic acid-containing drugs often suffer relatively high plasma drug clearance due to metabolism of the hydroxamate moiety, with glucuronide conjugate formation and aldehyde oxidase-mediated metabolism being common issues.¹⁶ A number of analogues in this series were evaluated in rats, and in all cases, moderate to high clearance was observed following iv dosing (Table 5). Glucuronide formation and aldehyde oxidase-mediated reduction of the hydroxamate moiety to the primary amide were determined to be major routes of metabolism (unpublished results). The metabolic liability of the hydroxamate moiety can be illustrated by comparing the rapid clearance observed with hydroxamate analogue **1v** (65 mL/min/kg) following iv dosing in rats to the relatively

Table 5. Rat Pharmacokinetic Data

compd	dose (mg/kg)	Cl (mL/min/kg)	V _{dss} (L/kg)	AUC (μg·h/mL)	T _{1/2} (h)
1a	10	58	2.7	2.8	3.2
1l	10	53	1.4	3.1	0.6
1v	10	65	2.6	2.5	1.4
1w	10	15	0.4	10.9	0.7

low clearance observed for the corresponding carboxylic acid **1w** (15 mL/min/kg).

In general, compounds in this series exhibit significant binding to human plasma protein (e.g., compound **1a**, HFu = 2%). A number of literature references suggest that a drug discovery strategy to lower human projected dose based on reducing plasma protein binding may be flawed, with the possible exception being programs focused on high clearance series with a need for iv drug delivery.¹⁷ The compounds described herein certainly exhibit moderately high clearance in rat, and iv delivery is a must-have for therapies targeting serious Gram-negative infections. Therefore, reducing protein binding became a goal for this medicinal chemistry program and design strategies to address this issue will be discussed in a subsequent publication.

To evaluate in vivo efficacy with compound **1a**, a murine acute systemic infection model was utilized. Mice were administered **1a** (subcutaneous dose; vehicle: 40% β-cyclodextrin in water) 0.5 and 4 h after an intraperitoneal challenge of *Pseudomonas aeruginosa* strain UC12120, a penicillin-resistant, quinolone-sensitive clinical isolate (**1a** MIC = 0.25 μg/mL). At 24 h postinfection, the animals were sacrificed and the bacterial burden in the spleen was determined. The drug dose providing 50% bacterial burden reduction relative to untreated animals (ED₅₀) was determined to be 35 mg/kg. Impressively, at a higher dose of 100 mg/kg, the spleen bacterial burden was reduced below the limits of detection (6.2 log burden reduction relative to control animals). An additional study was conducted wherein animal survival at 96 h post infection was utilized as the end point, thus providing a PD₅₀ = 63.4 mg/kg. In vivo dose fractionation studies conducted in a murine neutropenic thigh *Pseudomonas aeruginosa* infection model suggest that unbound AUC/MIC correlates best with efficacy for this drug class. While pharmacokinetic data was not gathered during the efficacy study described above for **1a**, extrapolation from a previous mouse pharmacokinetic study (50 mg/kg, subcutaneous) provides an unbound AUC/MIC ~ 8 for the PD₅₀ study.

CONCLUSION

Here we introduce a novel series of LpxC inhibitors which exhibit potent and selective enzyme inhibitory activity, broad spectrum whole-cell activity, and in vivo efficacy in a murine infection model. A key structural feature of this series is the methylsulfone-containing headgroup which engages in a key hydrogen-bonding interaction with the active site residue Lys238. Subsequent studies focused on optimizing the physical properties of this series to enable the identification of analogues worthy of advanced development will be discussed in a future publication.

EXPERIMENTAL SECTION

LpxC Enzyme Assay. The assay measures the enzymatic deacetylation of the synthetic lipid substrate UDP-3-*O*-(*R*-hydroxydecanoyl)-*N*-acetylglucosamine by mass spectrometry, using a

computer-controlled fluidic system combined with a triple quadrupole mass spectrometer (BioTrove RapidFire).¹⁸ The enzyme assay was conducted in 384 well polypropylene plates (Thermo 4312) in a total volume of 50 μL containing 100 pM purified *Pseudomonas aeruginosa* LpxC enzyme. The substrate buffer contains 100 mM Na₂PO₄, 1 mg/mL bovine serum albumin, pH 7.0. The enzyme buffer contains 5 mM Na₂PO₄ and 1.5 mg/mL bovine serum albumin, pH 7.5. Compounds (5 μL in 100% DMSO: compound final concentration range 100 μM to 1.0 pM) were preincubated with 20 μL of LpxC enzyme for 30 min at room temperature. The substrate UDP-3-*O*-(*R*-hydroxydecanoyl)-*N*-acetylglucosamine was added to initiate the assay, 25 μL at 1.0 μM (final concentration 0.5 μM). Assay plates were sealed, incubated at room temperature for 60 min, and the reaction was stopped by the addition of 10 μL of 1 N hydrochloric acid. The plates were read on the BioTrove RapidFire. Percent substrate conversion was calculated and plotted to obtain IC₅₀ values (at least *n* = 3 unless specified otherwise).

Antimicrobial Susceptibility Testing. The minimum inhibitory concentration (MIC) values were determined using the broth microdilution protocol according to the methods of the Clinical and Laboratory Standards Institute (CLSI). *Inoculum Preparation and Direct Colony Suspension:* Bacterial strains were grown on Tryptic soy agar with 5% sheep blood for 24 h prior to testing. Colonies of strains were suspended into sterile saline until a turbidity standard of 0.5 McFarland was achieved (approximately 1 × 10⁸ CFU/mL). This suspension was diluted 1:400 in Mueller–Hinton broth (2.5 × 10⁵ CFU/mL). *Drug Dilution Tray Preparation:* Compounds are diluted in appropriate solvent to 2200 μg/mL. The microbroth dilution stock plates were prepared in 2-fold dilution series, 64–0.06 μg drug/mL (high dilution series) and 0.25–0.00025 μg drug/mL (low dilution series). For tube 1 of the high dilution series, 200 μL of the 2220 μg/mL stock was added to duplicate wells of a 96-well microtiter plate. For tube 1 of the low concentration series, 200 μL of an 8.33 μg/mL stock was added to duplicate rows of a 96-well microtiter plate. Serial 2-fold decremental dilutions were made using a BioMek FX robot (Beckman Coulter Inc., Fullerton, California) with 10 of the remaining 11 wells, each of which contained 100 μL of the appropriate solvent/diluent. Row 12 contained solvent/diluent only and served as the control. Daughter plates were spotted (3.0 μL/well) from the stock plates listed above using the BioMek FX robot, yielding the final concentration of drug as described above. *Tray Inoculation:* Organisms were inoculated (100 μL volumes) using the BioMek FX robot. The final number of bacterial cells per well was approximately 2.5 × 10⁴ CFU/mL. The inoculated trays were placed in stacks of no more than 4 and covered with an empty tray. The trays were incubated for 16–20 h at 35 °C in an ambient air incubator. *MIC Test Results:* After inoculation and incubation, the degree of bacterial growth was estimated visually with the aid of a Test Reading Mirror (Dynex Technologies 220–16) in a darkened room with a single light shining directly through the top of the microbroth tray. The MIC was the lowest concentration of drug which prevented macroscopically visible growth under the conditions of the test. *Determining the MIC₅₀ and the MIC₉₀:* After all the MICs for each subset of strains were read, the values were sorted from highest to lowest and the MIC_{range}, MIC₅₀, and MIC₉₀ were calculated.

ASSOCIATED CONTENT

Supporting Information

Experimental details for compounds **1a–1x**, **3–7**, **9–14**, and **16–34**. This material is available free of charge via the Internet at <http://pubs.acs.org>. are available free of charge via the Internet at <http://pubs.acs.org>. Compound **1a** will be available to purchase from Sigma-Aldrich, Tocris, as well as Toronto Research Chemicals.

Accession Codes

The PDB code for compound **1t** is 3U1Y.

■ AUTHOR INFORMATION

Corresponding Author

*Phone: (860) 441-3522. E-mail: matthew.f.brown@pfizer.com.

■ ACKNOWLEDGMENTS

We thank David George, Lucinda Lamb, Deborah Gordon, and Judith Hamel for conducting infection model studies.

■ REFERENCES

- (1) Boucher Helen, W.; Talbot George, H.; Bradley John, S.; Edwards John, E.; Gilbert, D.; Rice Louis, B.; Scheld, M.; Spellberg, B.; Bartlett, J. Bad bugs, no drugs: no ESKAPE! An update from the Infectious Diseases Society of America. *Clin. Infect. Dis.* **2009**, *48* (1), 1–12.
- (2) Devasahayam, G.; Scheld, W. M.; Hoffman, P. S. Newer antibacterial drugs for a new century. *Expert Opin. Invest. Drugs* **2010**, *19* (2), 215–234.
- (3) Fischbach, M. A.; Walsh, C. T. Antibiotics for Emerging Pathogens. *Science* **2009**, *325* (5944), 1089–1093.
- (4) Payne, D. J.; Gwynn, M. N.; Holmes, D. J.; Pompliano, D. L. Drugs for bad bugs: confronting the challenges of antibacterial discovery. *Nature Rev. Drug Discovery* **2007**, *6* (1), 29–40.
- (5) Cipolla, L.; Polissi, A.; Airoidi, C.; Gabrielli, L.; Merlo, S.; Nicotra, F. New targets for antibacterial design: Kdo biosynthesis and LPS machinery transport to the cell surface. *Curr. Med. Chem.* **2011**, *18* (6), 830–852.
- (6) (a) Vaara, M. Outer membrane permeability barrier to azithromycin, clarithromycin, and roxithromycin in gram-negative enteric bacteria. *Antimicrob. Agents Chemother.* **1993**, *37* (2), 354–356. (b) Vuorio, R.; Vaara, M. The lipid A biosynthesis mutation lpxA2 of *Escherichia coli* results in drastic antibiotic supersusceptibility. *Antimicrob. Agents Chemother.* **1992**, *36* (4), 826–829.
- (7) Young, K.; Silver, L. L.; Bramhill, D.; Cameron, P.; Eveland, S. S.; Raetz, C. R. H.; Hyland, S. A.; Anderson, M. S. The envA permeability/cell division gene of *Escherichia coli* encodes the second enzyme of lipid A biosynthesis. UDP-3-O-(R-3-hydroxymyristoyl)-N-acetylglucosamine deacetylase. *J. Biol. Chem.* **1995**, *270* (51), 30384–30391.
- (8) Onishi, H. R.; Pelak, B. A.; Gerckens, L. S.; Silver, L. L.; Kahan, F. M.; Chen, M.-H.; Patchett, A. A.; Galloway, S. M.; Hyland, S. A.; et al. Antibacterial agents that inhibit lipid A biosynthesis. *Science* **1996**, *274* (5289), 980–982.
- (9) (a) Barb, A. W.; Zhou, P. Mechanism and inhibition of LpxC: an essential zinc-dependent deacetylase of bacterial lipid A synthesis. *Curr. Pharm. Biotechnol.* **2008**, *9* (1), 9–15. (b) Cuny, G. D., A new class of UDP-3-O-(R-3-hydroxymyristol)-N-acetylglucosamine deacetylase (LpxC) inhibitors for the treatment of Gram-negative infections: PCT application WO 2008027466. *Expert Opin. Ther. Pat.* **2009**, *19*(6), 893–899; (c) Faruk Mansoor, U.; Vitharana, D.; Reddy, P. A.; Daubaras, D. L.; McNicholas, P.; Orth, P.; Black, T.; Arshad Siddiqui, M. Design and synthesis of potent Gram-negative specific LpxC inhibitors. *Bioorg. Med. Chem. Lett.* **2011**, *21* (4), 1155–1161. (d) Liang, X.; Lee, C.-J.; Chen, X.; Chung, H. S.; Zeng, D.; Raetz, C. R. H.; Li, Y.; Zhou, P.; Toone, E. J. Syntheses, structures and antibiotic activities of LpxC inhibitors based on the diacetylene scaffold. *Bioorg. Med. Chem.* **2011**, *19* (2), 852–860. (e) Barb, A. W.; Leavy, T. M.; Robins, L. I.; Guan, Z.; Six, D. A.; Zhou, P.; Bertozzi, C. R.; Raetz, C. R. H. Uridine-based inhibitors as new leads for antibiotics targeting *Escherichia coli* LpxC. *Biochemistry (Moscow)* **2009**, *48* (14), 3068–3077.
- (10) (a) Cole, K. E.; Gattis, S. G.; Angell, H. D.; Fierke, C. A.; Christianson, D. W. Structure of the Metal-Dependent Deacetylase LpxC from *Yersinia enterocolitica* Complexed with the Potent Inhibitor CHIR-090. *Biochemistry (Moscow)* **2011**, *50* (2), 258–265. (b) Whittington, D. A.; Rusche, K. M.; Shin, H.; Fierke, C. A.; Christianson, D. W. Crystal structure of LpxC, a zinc-dependent deacetylase essential for endotoxin biosynthesis. *Proc. Natl. Acad. Sci. U.S.A.* **2003**, *100* (14), 8146–8150. (c) Mochalkin, I.; Knafels, J. D.; Lightle, S. Crystal structure of LpxC from *Pseudomonas aeruginosa* complexed with the potent BB-78485 inhibitor. *Protein Sci.* **2008**, *17* (3), 450–457. (d) Coggins, B. E.; McClerren, A. L.; Jiang, L.; Li, X.; Rudolph, J.; Hindsgaul, O.; Raetz, C. R. H.; Zhou, P. Refined Solution Structure of the LpxC-TU-514 Complex and pK_a Analysis of an Active Site Histidine: Insights into the Mechanism and Inhibitor Design. *Biochemistry (Moscow)* **2005**, *44* (4), 1114–1126.
- (11) Anderson, G. M. III; Kollman, P. A.; Domelsmith, L. N.; Houk, K. N. Methoxy group nonplanarity in *o*-dimethoxybenzenes. Simple predictive models for conformations and rotational barriers in alkoxyaromatics. *J. Am. Chem. Soc.* **1979**, *101* (9), 2344–2352.
- (12) Kalgutkar, A. S.; Obach, R. S.; Maurer, T. S. Mechanism-based inactivation of cytochrome P450 enzymes: chemical mechanisms, structure–activity relationships and relationship to clinical drug–drug interactions and idiosyncratic adverse drug reactions. *Curr. Drug Metab.* **2007**, *8* (5), 407–447.
- (13) Lomovskaya, O.; Zgurskaya, H. I.; Totrov, M.; Watkins, W. J. Waltzing transporters and “the dance macabre” between humans and bacteria. *Nature Rev. Drug Discovery* **2007**, *6* (1), 56–65.
- (14) Chuanchuen, R.; Beinlich, K.; Hoang, T. T.; Becher, A.; Karkhoff-Schweizer, R. R.; Schweizer, H. P. Cross-resistance between triclosan and antibiotics in *Pseudomonas aeruginosa* is mediated by multidrug efflux pumps: exposure of a susceptible mutant strain to triclosan selects nfxB mutants overexpressing MexCD-OprJ. *Antimicrob. Agents Chemother.* **2001**, *45* (2), 428–432.
- (15) Screen was performed by Cerep Corp. 15318 NE 95th St. Redmond, WA 98052, USA; www.cerep.com.
- (16) Dalvie, D.; Cosker, T.; Boyden, T.; Zhou, S.; Schroeder, C.; Potchoiba, M. J. Metabolism distribution and excretion of a matrix metalloproteinase-13 inhibitor, 4-[4-(4-fluorophenoxy)-benzenesulfonylamino]tetrahydropyran-4-carboxylic acid hydroxyamide (CP-544439), in rats and dogs: assessment of the metabolic profile of CP-544439 in plasma and urine of humans. *Drug Metab. Dispos.* **2008**, *36* (9), 1869–1883.
- (17) (a) Benet, L. Z.; Hoener, B.-A. Changes in plasma protein binding have little clinical relevance. *Clin. Pharmacol. Ther.* **2002**, *71* (3), 115–121. (b) Smith, D. A.; Di, L.; Kerns, E. H. The effect of plasma protein binding on in vivo efficacy: misconceptions in drug discovery. *Nature Rev. Drug Discovery* **2010**, *9* (12), 929–939.
- (18) Langsdorf, E. F.; Malikzay, A.; Lamarr, W. A.; Daubaras, D.; Kravec, C.; Zhang, R.; Hart, R.; Monsma, F.; Black, T.; Ozbil, C. C.; Miesel, L.; Lunn, C. A. Screening for antibacterial inhibitors of the UDP-3-O-(R-3-hydroxymyristoyl)-N-acetylglucosamine deacetylase (LpxC) using a high-throughput mass spectrometry assay. *J. Biomol. Screening* **2010**, *15* (1), 52–61.